

Nano-structural characterizations: Elongation of graphene layers within solid hydrocarbons

Kamel A. K. Gadallah^{*1}

¹Astronomy Department, Faculty of Science, Al-Azhar University, Nasr City, PO Box 11884 Cairo, Egypt

**Original research
papers**

Received: XX December 20XX

Accepted: XX December 20XX

Online Ready: XX December 20XX

Abstract

Nano-structural characterizations of solid hydrocarbons were explained during their formation by the laser ablation technique and during the heat treatment. For the hydrogenated amorphous carbon (HAC), these characterizations cover the hydrogen content, the sp^3 and sp^2 hybridization, the band gap energy, and the length of the graphene layers. In the atomic and electronic structure of HAC, the hydrogen to carbon and sp^3 to sp^2 ratios were characterized through the C-H stretching vibration in the mid-IR band at around the 2924 cm^{-1} . An increase in the optical band gap energy and in the length of the graphene layers in a nano-sized scale was observed with the laser power. After heat treatments of HAC, hydrogen content, sp^3/sp^2 ratio and the band gap decrease while the average length of the graphene layers increases. Higher laser power shows elongation of the graphene layers in the hydrogen-rich HAC while heat treatments show this in the hydrogen-poor HAC.

Keywords: amorphous carbon; nano-structure; plasma deposition; heat treatment; infrared spectroscopy

1 Introduction

A hydrocarbon material with dependence of sp^1 , sp^2 and sp^3 hybridization on the H/C ratio is known as Hydrogenated Amorphous Carbon (HAC). In the literature, this material is often abbreviated to a-C:H. Within HAC, there is a substantial degree of the medium-range order up to (2-3) nm and both sp^2 and sp^3 sites are somewhat separated and clustered. The short-range order results from the local

^{*}Corresponding author: E-mail: Kamel.Gadallah71@gmail.com

chemical bonding of the atoms and concerns the spatial coordination of the carbon atoms, which are recognized by the sp^3/sp^2 ratio. This ratio can be measured by some spectroscopic methods such as nuclear magnetic resonance Pan et al. (1991), Near Edge X-Ray Absorption Fine Structure Berger et al. (1988), and electron energy loss spectroscopy Jäger et al. (1999). The material, which has $sp^3/sp^2 > 1$, is a more diamond-like material, whereas the material, which has $sp^3/sp^2 < 1$, is a more graphite-like material. The description of more graphitic and conducting materials (in a medium-range order) depends on the arrangement of sp^2 sites in aromatic islands. These islands are often called basic structural units or BSUs Jäger et al. (1999); Mikhailov et al. (2001). BSUs can be piled up in nano-sized packets of 2-4 graphene layers. They can be found between clusters having much amount of sp^3 hybridization with a straight or bent structure. The medium-range order can be observed in HAC by the transmission electron microscopy (TEM) Green and McKenzie (1990) and scanning tunneling microscopy (STM), Marchon et al. (1989).

More sp^3 sites, which take place through an exothermic reaction, show the role of hydrogen in forming $=C-H$, $-C-H_{2,3}$ groups in the HAC network. These groups are responsible for the observed absorption of such compounds near 3030 cm^{-1} and 2924 cm^{-1} , respectively. The structural and optical properties of HAC such as the sp^3/sp^2 ratio, the band gap energy and the length of the graphene layers depend mainly on the hydrogen content (H/C). Where the coordination of carbon atoms with hydrogen is only assumed in sp^3 and sp^2 hybridization bondings in the HAC network ignoring the very small sp^1 fraction. As much hydrogen fraction is incorporated in HAC, more aliphatic structures are formed, due to the higher sp^3 sites, showing strong C-H stretching modes with higher mass absorption coefficient in the 2924 cm^{-1} region (Gadallah et al., 2011). The H/C and sp^3/sp^2 ratios can be easily under control, hence the structural and optical properties of the HAC-film. Increasing sp^3 sites leads to the increase of the optical gap energy. In Dischler (1987), the hydrogen content in HAC materials is critically controlled by the initial physical conditions of the formation process and it also decreases by annealing above about $300\text{ }^\circ\text{C}$.

In laboratory astrophysics during the last few decades, a variety of methods were taken into account to produce HAC films in nano-sized scale. Such methods are the mass-selected ion beam deposition (MSIB) Aksentiv et al. (1980), arc discharge in air and H_2 atmosphere Colangeli et al. (1992); Zubko et al. (1996), rf sputtering Li and Lannin (1990), plasma-enhanced chemical vapor deposition (PECVD) Mutsukura et al. (1992); Furton et al. (1999), resistive heating of graphite electrodes Schnaiter et al. (1998); Jäger et al. (1999), laser plasma deposition Davanloo et al. (1990), and laser ablation in gaseous atmospheres Grishko and Duley (2002); Duley and Lazarev (2004); Jäger et al. (2008); Gadallah et al. (2011, 2012a). In the astrophysical-implications, HAC materials produced by laser ablation have been considered as laboratory analogs of the carbonaceous cosmic dust Gadallah et al. (2011, 2012a, 2013) and as carriers of the interstellar UV bump at 217.5 nm Gadallah et al. (2012b) in the interstellar medium. In astrophysical implications, the required structural and optical properties of HAC are in relevance to the hydrogen fraction within HAC. In the current study, both the laser power and heat treatments of HAC are considered to study the influences on the nano-structural behavior.

2 Analytical techniques

TEM images, which were obtained by a JEOL JEM-3010 microscope equipped with a LaB_6 cathode working at an acceleration voltage of 300 kV , provide more information about the particle's shape and size. The internal structure of carbonaceous material can be described by these images in high-resolution modes. Studies by Jäger et al. (1998, 2008) and Mikhailov et al. (2001) showed that carbonaceous nanoparticles consist of small spherical primary particles having sizes between a few and tens of nanometers. Frequently, they are incorporated in branched aggregates. TEM images can clearly show that these particles are composed of the bent graphene layers with various lengths and interlayer distances. Here, the Gatan Digital Micrograph program is used to measure manually the

average length (L_a) of the graphene layers.

Fourier transform IR (FTIR) spectroscopy in the mid-IR range allows us to clarify the electronic and atomic structures of HAC which is affected by the incorporated hydrogen. The H/C ratio can be derived from spectroscopic way from the integrated area under the C-H stretching bands around 2924 cm^{-1} Angus and Jansen (1988); Gadallah et al. (2011). The sp^3/sp^2 ratio can be estimated using the expression,

$$\frac{\text{sp}^3}{\text{sp}^2} = \frac{6X_H - 1}{8 - 13X_H} \quad (2.1)$$

where $X_H = (\text{H/C})/(1+\text{H/C})$. Equation (2.1) was derived by Angus and Jansen (1988), using an approach of a random covalent network given by Phillips (1979). This equation is only valid for X_H between 17 and 62% and the accuracy of the calculation of the sp^3/sp^2 ratio is dependently linked to those of the H/C ratio in range of 10% of error too.

For an amorphous semiconductor material such as a HAC material, optical absorption measurements in the NIR-FUV range provide information about the optical band gap energy, E_g , which is estimated from the Tauc relation

$$\sqrt{\alpha E} = B(E - E_g) \quad (2.2)$$

where α is the linear attenuation coefficient, E is the photon energy, and B is a constant. E_g and the slope B are related to the range of the aromatic cluster size in the HAC materials (Robertson and O'Reilly, 1987). This relation is mostly used in the laboratory to determine the gap energy of materials prepared by thin-film or particle deposition.

3 Experimental

To produce HAC samples in nano-sized scale by the laser ablation, a Nd:YAG laser with very short and intense pulses at a wavelength of 532 nm (second harmonic) was used. The ablation took place in a quenching gas atmosphere (He and H_2) at a pressure of 4.5 mbar. A supersonic expansion of the hot plasma leads to the condensation of carbon particles. During the evaporation process, the laser beam hits a solid surface of a graphite target and vaporizes very small quantities of carbons as intense plasma. The laser ablation technique is characterized by the laser power (F_l), which was controlled by the area of the laser beam focus on the target. The duration of the laser pulses, t , was 10 ns with pulse energy E_{pulse} of 250 mJ. The laser power was determined by the following equations,

$$F_l = \frac{E_{\text{pulse}}}{t\pi r^2} \quad (3.1)$$

where r is the radius of the focused area of the laser beam. In the present experiment, the value of F_l was $2 \times 10^8\text{ Wcm}^{-2}$ in the case of low-focused laser beam (with $r \approx 1\text{ mm}$). This value gave a vibrational temperature of 4000 K in the condensation zone Jäger et al. (2008). To increase the hydrogen content of produced HAC, we increased the laser power by approximately two orders of magnitude in the case of a high-focused laser beam (with $r \approx 0.15\text{ mm}$). Higher laser power rises vibrational temperature of laser-induced plasma higher than 4000 K Iida and Yeung (1994), leading to more dissociative carbon atoms and even small carbon molecules. Consequently in this environment, the dissociative hydrogen and carbon atoms are plentiful gas-phase precursors to form the olefinic and aliphatic molecules in $\text{CH}_{2,3}$ groups. F_l has been derived from measuring the average power with a powerlite meter (Continuum C5100) ranging from 1 to 2.2 Watt (for a laser pulse rate of 10 Hz). Samples were produced at two different values of F_l , as shown in Table 1. Samples from S1 to S8 were produced at low laser power (LLP) while others from S9 to S16 were produced at high laser power (HLP).

In the experimental setup, four chambers (for evaporation, expansion, analyzing and deposition) were used to produce HAC materials, according to Jäger et al. (2008). To avoid strong structural processing and agglomeration of the original condensed materials, particles passed to the condensation

zone in the evaporation chamber through the nozzle and skimmer. A freely propagating particle beam was formed throughout the low-pressure atmosphere in the expansion and analyzing chambers. Quenching gases (He and H₂) were continuously supplied because of the loss through the nozzle to the expansion chamber, which was continuously pumped. The gas flows were controlled by a “multi gas controller 647B (MKS)”. Then materials have been deposited in a separated chamber (deposition chamber) in high vacuum of pressure of $(5 \pm 3) \times 10^{-6}$ Torr. The amount of deposited carbon materials i.e. the film thickness, d , on the substrate (SiO₂, CaF₂, or KBr substrates) has been estimated by means of a quartz microbalance, on which a part of the cross section of the particle beam was fallen. The thickness was corrected to the coverage area on the microbalance. Finally, in the condensation zone at a pressure of 4.5 mbar, collisions between the evaporated carbon atoms and also between clusters and all of these with the quenching gas (He/H₂) in a supersonic expansion of the hot plasma caused the condensation of carbon particles. Physical conditions used to prepare samples and analytical results are given in Table 1.

The thermal processing of HAC could be helpful to understand the modification of properties of HAC in hot media. In this experiment, some samples were heated at different temperature in the same chamber of the deposition in high vacuum (approximately 10^{-6} Torr). In this method, the heating process was achieved using an electrical heating system connected in the substrate chamber. A thermocouple connected with the sample holder inside the substrate chamber was used to measure the temperature of the sample. In this system, the temperature was controlled to go slowly up to 50 °C and remain constant for at least one hour to remove some radicals of hydrocarbons present inside the chamber. It was also kept constant at 200 °C for two hours or more to let chemical adsorbates go outside by pumping. The results of the effect of heating on the electronic and atomic structures of HAC are listed in Table 1.

4 Results and discussion

The study of structural and optical properties of HAC is necessary to understand the modification of their internal structure as a function of the laser power. A change in the laser power leads to a change in the temperature of the plasma in the condensation zone. Consequently, changes in H/C and sp³/sp² ratios, L_a , and Tauc gap energy, E_g , of produced carbonaceous nanoparticles take place. Heat treatments of HAC affect these properties too. In the next subsections, the analytical techniques of TEM images are presented. Elongation in the average length of the graphene layers has been observed by increasing laser power and temperature.

4.1 TEM of HAC materials

Changing the laser power leads to differences in the structure of the deposit, as shown in Figure 1. Inspection of TEM images shows that more pores are observed at using LLP as shown in panels (a), (b) and (c). On the other hand in panel (d), the structure obtained by HLP is very dense and no pores inside the material are observed. This is most likely due to higher evaporation of carbon atoms and high-condensation rate of hydrocarbons formed with the stronger laser power. The deposited grains shown in panels (a), (b) and (c) are of small-size range (2-4 nm) whereas the grain size of the material shown in panel (d) is not clear because it is very dense. In panels (a), (b) and (d), the agglomerates are mostly fragments of fullerenes and chain-like agglomerates of carbon grains. For the material (S2) in the panel (c), it seems that the agglomerates are mostly in closed fullerene-like carbon materials. It might be due to the lower fraction of incorporated hydrogen in the production conditions (quenching gases) compared with those of the material (S1) in panels (a and b) since S1 and S2 samples were produced at the same LLP. A typical appearance of the strongly bent and disordered graphene layers and small fullerene-like carbon grains is observed in all materials. Elongation indicating graphitization within HAC was observed in the graphene layers with the laser power in spite of the presence of high

Table 1: Physical conditions to produce HAC samples in a gas pressure equal to 4.5 Torr and analytical results.

S# ¹	d nm	He: H ₂	F _I Wcm ⁻²	Before heating				Heat treatments				
				L _a nm	H/C	sp ³ /sp ²	E _g eV	T °C	L _a nm	H/C	sp ³ /sp ²	E _g eV
S1	75	50:30	2×10 ⁸	0.42	0.60	0.40	1.1	100	1.1
								300	1.04
								420	1.02
S2	27	50:15	2×10 ⁸	0.45	1.2
S3	38	50:30	2×10 ⁸	0.62	0.43	1.21
S4	25	50:15	2×10 ⁸	1.42
S5	30	50:30	2×10 ⁸	1.5
S6	58	50:30	2×10 ⁸	0.61	0.41	1.55
S7	117	50:30	2×10 ⁸	0.60	0.40	50	0.55	0.33
								200	0.45	0.21
								300	0.33	0.11
								350	1.8	0.11
S8	125	50:30	2×10 ⁸	0.61	0.41	50	0.53	0.30
								200	0.41	0.18
								434	0.00
S9	65	90:20	2.8×10 ¹⁰	0.70	0.55	1.65	300	1.4
								430	1.1
S10	40	80:20	2.1×10 ¹⁰	0.79	0.74	1.7
S11	40	80:20	1.4×10 ¹⁰	0.69	0.55	1.8
S12	75	90:20	2.8×10 ¹⁰	0.72	0.77	0.69	1.82
S13	25	50:20	3.0×10 ¹⁰	2.15
S14	120	90:20	2.8×10 ¹⁰	0.82	0.80
S15	93	90:10	2.8×10 ¹⁰	0.79	0.70	50	0.83	0.81
								200	0.79	0.73
								327	0.7	0.56
S16	91	50:20	3.1×10 ¹⁰	0.75	0.65	430	2.0	0.1
							

Note:⁽¹⁾S13, S14, and S15 were deposited on a CaF₂ substrate, while S7, S8 and S16 were deposited on a KBr substrate. Others were deposited on a SiO₂ substrate. S1, S2, S7, S12, S15 were used for TEM.

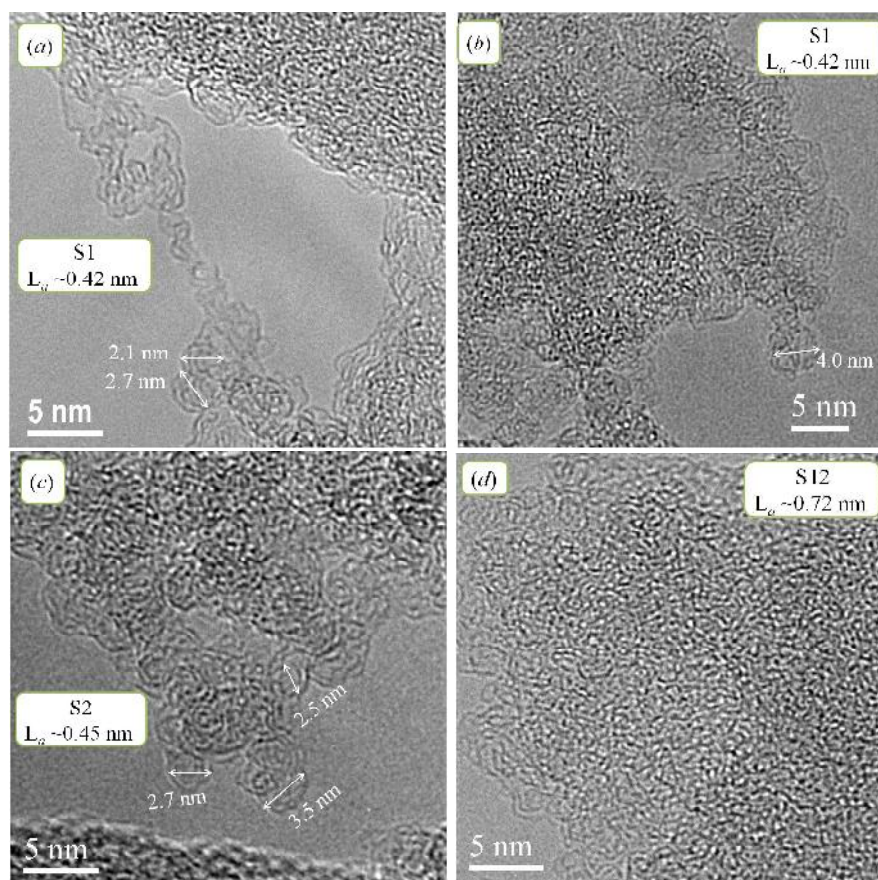


Figure 1: TEM images of HAC; S1 (panels a and b) and S2 (panel c) were produced by using LLP while S12 (panel d) was produced by using HLP.

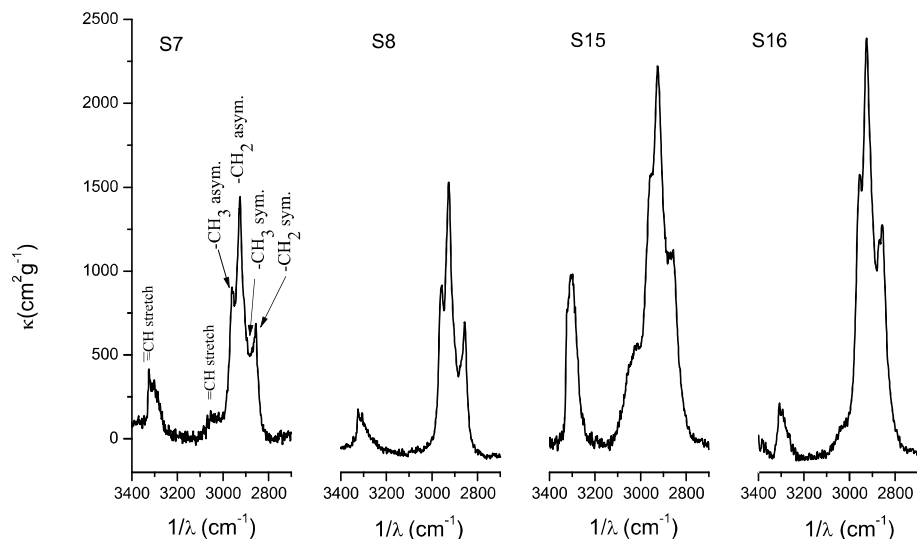


Figure 2: Mid-IR spectra of samples produced by using LLP (S7 and S8) and of those produced by using HLP (S15 and S16) in the laser ablation.

hydrogen content. L_a is roughly between 0.42 nm at using LLP and 0.72 nm at using HLP. However very longer graphene layers are rarely observed and they were excluded.

4.2 H/C, sp^3/sp^2 ratios and E_g versus the laser power

By using LLP, the deposition rate of the particles is approximately 1.6 ± 0.4 nm/min while it reaches 2.5 ± 0.5 nm/min by using HLP. With increasing the laser power to the maximum value, the highly focused laser beam forms a very bright and big plume of plasma, leading to the formation of more carbon atoms. Consequently, such atoms are bonded together and with hydrogen atoms in different functional groups of hydrocarbons such as in $\equiv C-H$, in aromatic $=C-H$ or saturated aliphatic $-CH_{2,3}$ groups. In Figure 2, the mid-IR spectra show strong $-C-H$ stretching band at 2924 cm^{-1} with a high mass absorption coefficient (κ). This band increases with the laser power. An additional recognized band of $=C-H$ at 3020 cm^{-1} and another of $\equiv C-H$ band at 3300 cm^{-1} are also observed. The 3020 cm^{-1} $=C-H$ band is generally weak when the structure of HAC is mostly dominated by aliphatic structures. This band appears remarkably in samples S7, S15 and S16 although it seems very weak in S16 relative to the aliphatic C-H bands and sometimes it disappears as in case of S8.

The trend of fitting the H/C ratio shows an increase with the laser power, as shown in Figure 3. It is probably attributable to the formation of aliphatic and olefinic $CH_{2,3}$ groups due to the more dissociative carbon atoms in the higher-temperature plasma. These groups link between the fullerene fragments causing a simultaneous increase of the aliphatic CH stretching modes close to the 2924 cm^{-1} band. In this case, the formation of aliphatic and/or olefinic hydrocarbon chains is also predicted close to the 3020 cm^{-1} band, in particular in the spectra of S15, as shown in Figure 2. These chains might appear in bridges located between aromatic compounds in HAC materials (produced with HLP). The H/C ratio increases due to the higher aliphatic and olefinic hydrocarbon bridges because

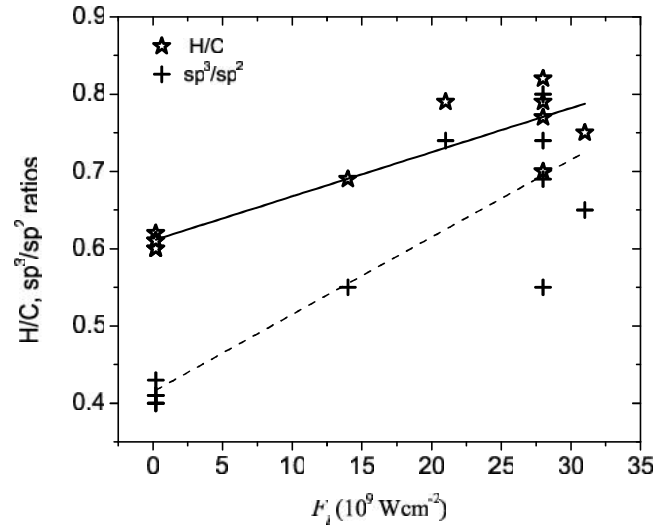


Figure 3: H/C and sp^3/sp^2 ratios versus of the laser power.

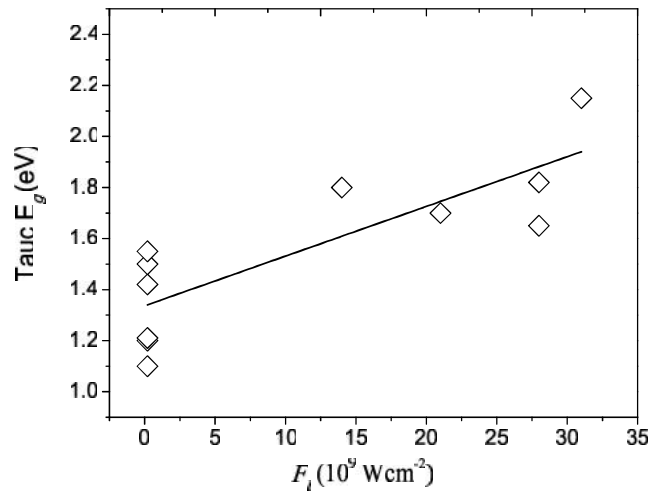


Figure 4: Tauc gap energy, E_g (eV), of some samples of HAC versus the laser power, F_l (10^9 Wcm^{-2}).

materials in S15 are very condensed. In Figure 3, the direction of fitting the sp^3/sp^2 ratio is mainly in correlation with the hydrogen fraction so it increases also with the laser power. Finally it is concluded that using the HLP to produce HAC increases the fraction of the C-H bonds, which are bonded also in double and triple forms with carbon atoms due to the increasing of the sp^2 and sp^1 hybridization, respectively.

From the results in Table 1, the gap energy is in the range between 1.1 eV and 1.55 eV for S1-S6, produced with LLP, and between 1.65 eV and 2.15 eV for S9-S13, for HLP. The fitting line in Figure 4 shows the trend of the gap energy, which increases proportionally with the laser power.

In the literature, the H/C and sp^3/sp^2 ratios and the gap energy agree with those of a HAC produced by plasma enhanced chemical vapor deposition (PECVD) Furton et al. (1999), in which these ratios are 0.5 of both and the gap energy is 1.9 eV. For a similar material to HAC, the tetrahedral amorphous carbon (ta-C), produced by pulsed laser deposition Miyajima et al. (2009), has different structural properties (high fraction of $sp^3/sp^2 > 2$ and low band gap energy below 1 eV) than those of HAC. In the study of the ta-C by Miyajima et al. (2009), the effect of the laser power gives an increase of sp^3 and the deposition rate of the ta-C. In agreement, this effect gives a similar trend of sp^3 and the deposition rate of the HAC. On the other hand, for the ta-C with the increase of the laser power, the band gap energy is unlikely below 1 eV for a material containing highly sp^3 fractions.

4.3 Heat treatment of HAC materials

The structure of HAC materials is very sensitive to the thermal annealing. Under specific conditions seen in Table 1, heat treatments were done in high vacuum for some samples (Section 3).

TEM images seen in Figure 5 show the evolution of the structure with annealing at temperatures of 100, 350 and 450 °C as shown in panels (a), (b) and (d) respectively. L_a increases from 0.42 nm at room temperature to 2.0 nm at 430 °C. In S7, some graphitic fibers are observed at higher temperatures. In panel (c), S7 was heated up to 350 °C, in which a partial graphitization results from the inhomogeneous heating of the materials. Generally, TEM images reveal the modification of the structure of HAC by the thermal annealing and an increase of the average length of the graphene layers is observed.

Spectra of S7, S8 and S15 show that they originally have different mass absorption coefficients in the mid-IR band, and indeed they are affected by annealing, losing most of the hydrogen content. The mass absorption coefficient is very sensitive to the higher temperature, as shown in the left panels of Figure 6. The C-H stretching band in the 3000-2800 cm^{-1} range and the $\equiv C-H$ stretching band at 3300 cm^{-1} vanish at temperatures between 350 and 434 °C. It seems that the hydrogen content decreases with annealing. The dependence of the H/C and sp^3/sp^2 ratios on annealing temperature is shown in the right panels of Figure 6. It is correlated to the integrated area of the mass absorption coefficient at the C-H stretching band (left panels), so the H/C and sp^3/sp^2 ratios decrease as the annealing temperature increases. Comparing the behavior of H/C and sp^3/sp^2 ratios with heating for S7 and S8 with the behavior of those for S15, the ratios decline faster in case S7 and S8 than those in case S15. For S15, the hydrogen content increases with heating, at the lower temperatures. Higher temperatures are required to remove adsorbates of hydrocarbons which are attached on the carbonaceous grains. In particular, these deposits produced at HLP are denser than those produced at LLP. For this sample, the H/C ratio decreases slowly up to $T=327$ °C. After that it decreases sharply with the higher temperature. This is probably because of losing most of the hydrogen fraction at $T > 430$ °C. It is recognized that the $\equiv C-H$ stretching band at 3020 cm^{-1} is not reduced by heat treatments but it has become slightly stronger. With heating, as the aromatic structures dominate HAC, this band becomes stronger relative to the aliphatic C-H bands in the CH stretching region as shown in Figure 6. It is particularly observed in the spectra of sample S8 with heating at 200 and 434 °C whereas this sample does not show this band before heating. In the study by Goto et al. (2000, 2003) for a similar material and as an evidence for the dominant aromatic structures, the 3020 $cm^{-1} \equiv C-H$ band becomes the dominant with annealing. The estimated sp^3/sp^2 ratio from equation (2.1) is limited to

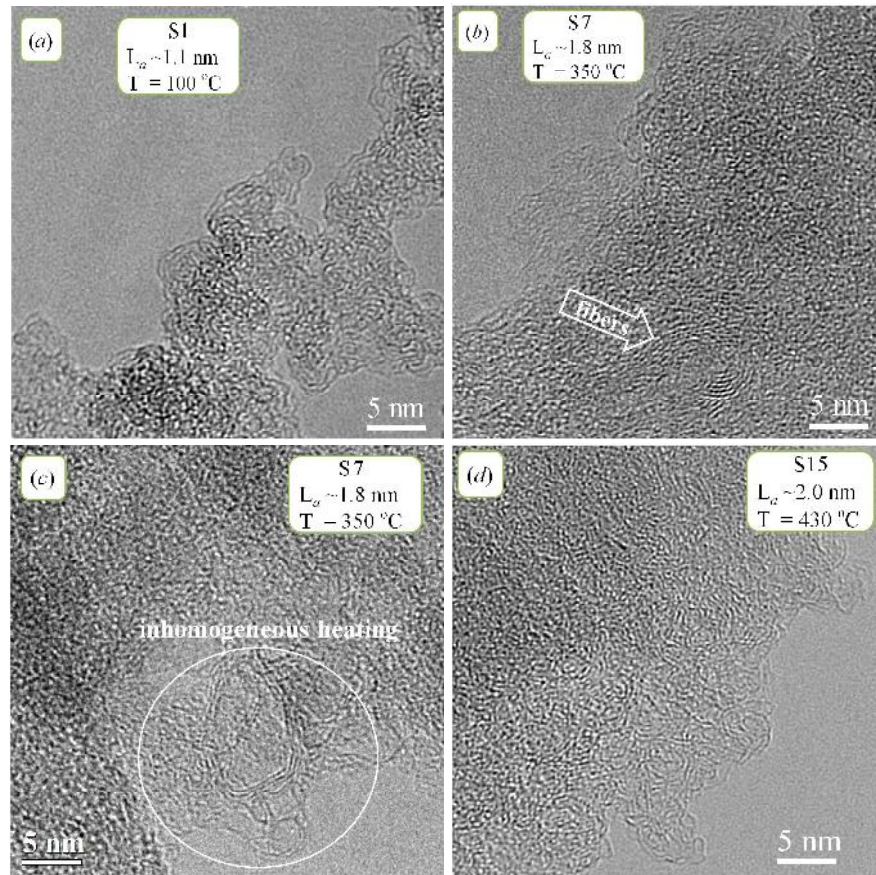


Figure 5: TEM images of HAC after heat treatments: S1 (panel a) was heated up to 100 °C while S7(panels b and c) was heated up to 350 °C and S15 (panel d) was heated up to 430 °C.

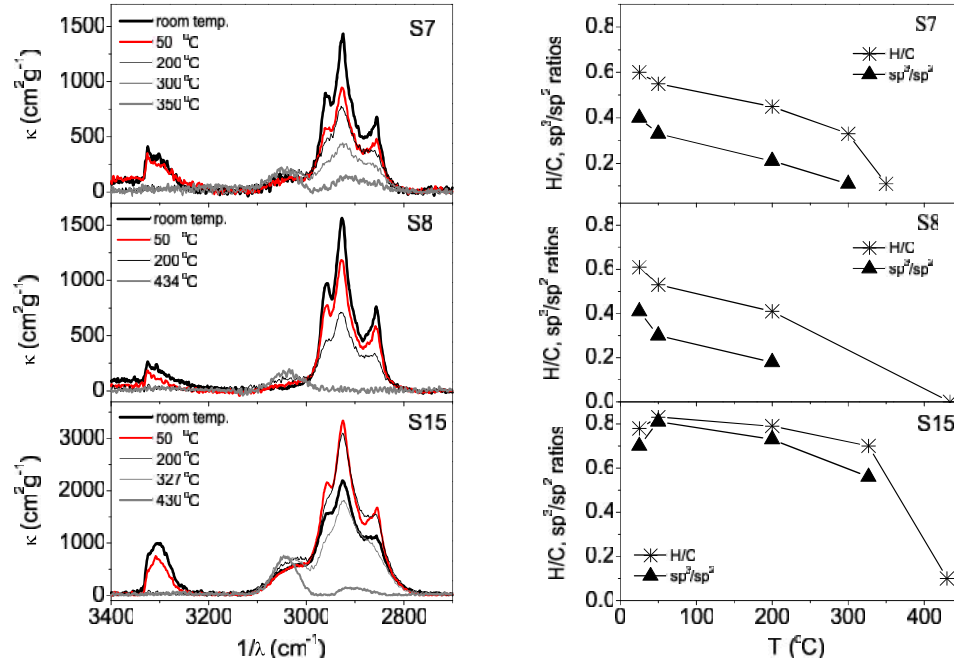


Figure 6: Mid-IR spectra (left panels) and H/C and sp^3/sp^2 ratios (right panels) as a function of temperatures of S7, S8 and S15 before and after heat treatments.

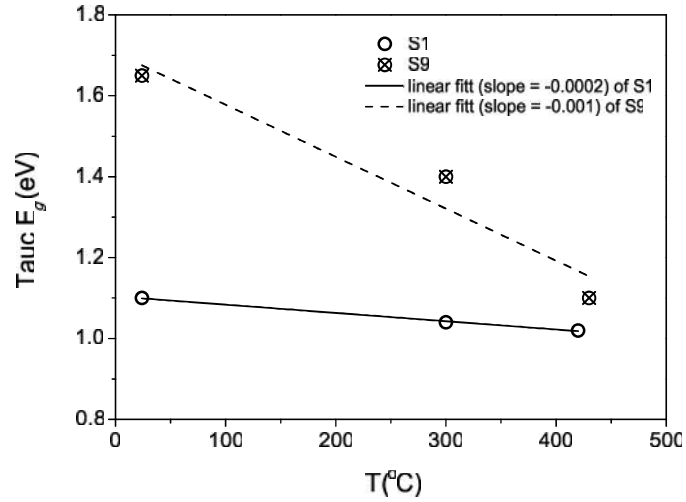


Figure 7: Tauc gap energy, E_g (eV), as function of temperatures of S1 and S9 samples before and after heat treatments.

the range of H/C ratio mentioned above. Therefore, there is a lack of some values of the sp^3/sp^2 ratio at high temperature due to the very small value of the H/C ratio.

As well, the gap energy of HAC decreases as the annealing temperature increases, as shown in Figure 7. Where it is conversely in relevance to the average length of the graphene layers (Robertson, 1991), the decrease in the gap energy is attributed to the increase in aromatic clustering of sp^2 sites. The fraction of these sites in principle increases with the annealing temperature due to the loss of hydrogen atoms (Mennella et al., 1995). Figure 7 shows two linear fittings with different slope (-0.0002 and -0.001 for S1 and S9, respectively). The linear fitting of S9 declines faster than those of S1 because S9 has gap energy and hydrogen content higher than those in S1. For S1, when the temperature reaches 420 °C, the Tauc E_g value decreases slowly from 1.1 to 1.02 eV. For S9, when the temperature increases to 430 °C, it declines more strongly from 1.65 to 1.1 eV.

5 CONCLUSIONS

In the laser ablation technique, an increase in the laser power evaporates more carbon species in the condensation zone with high-temperature plasma. Consequently, it results in a change in the characteristics of HAC. These characteristics are explained analytically by TEM and spectroscopic properties. TEM images show that the grain size in the deposited HAC lays between 2 and 4 nm and the average length of the graphene layers increases with providing HLP. Analytical results in the mid-IR spectral ranges shows that the hydrogen content of the deposit condensed in He/H₂ atmosphere can be controlled by the laser power density. It reaches higher values between 60 and 80 percent when HLP is used. The sp^3/sp^2 hybridization ratio is correlated to the hydrogen content. The value of the gap energy E_g derived from the Tauc relation lies in the range from 1.1 to 2.15 eV corresponding to the range from lower to higher values of the laser power, respectively. As a result, all these characteristics of HAC increase with improving the laser power. The characteristics are reduced as the heat treatments increase. The average length of the graphene layers, however, increases.

Acknowledgment

This work was financially supported by the Science & Technology Development Fund (STDF), Egypt. I am grateful to the laboratory group at Astrophysical Institute and University Observatory, Friedrich Schiller University Jena, Germany, in particular Harad Mutschke and Cornilia Jäger for giving me the chance to achieve this work. I would also thank Prof. M. Elokr from Al-Azhar University for the useful cooperation.

References

- Akseniv, I.I., Vakula, S.I., Padalka, V.G., Strenlitski, R.E., Khoroshikh, V.M., 1980. Soviet Phys. Tech. Phys. 25, 1164.
- Angus, J.C., Jansen, F., 1988. Dense “diamondlike” hydrocarbons as random covalent networks. Journal of Vacuum Science Technology 6, 1778–1782.
- Berger, S.D., McKenzie, D.R., Martin, P.J., 1988. EELS analysis of vacuum arc-deposited diamond-like films. Philosophical Magazine Letters 57, 285–290.
- Colangeli, L., Blanco, A., Fonti, S., Bussoletti, E., 1992. Vacuum ultraviolet extinction measurements on cosmic dust analog carbon grains. Astrophysical Journal 392, 284–288.

- Davanloo, F., Juengerman, E.M., Jander, D.R., Lee, T.J., Collins, C.B., 1990. Amorphous diamond films produced by a laser plasma source. *Journal of Applied Physics* 67, 2081–2087.
- Dischler, B., 1987. Amorphous hydrogenated carbon films, Ed. P. Koidland and P. Oelhaven. *Proc. Euro. Mat. Res. Soc., Les Editions de physique*, Paris, 17, 189.
- Duley, W.W., Lazarev, S., 2004. Ultraviolet Absorption in Amorphous Carbons: Polycyclic Aromatic Hydrocarbons and the 2175 Å Extinction Feature. *Astrophysical Journal, Letters* 612, L33–L35.
- Furton, D.G., Laiho, J.W., Witt, A.N., 1999. The Amount of Interstellar Carbon Locked in Solid Hydrogenated Amorphous Carbon. *Astrophysical Journal* 526, 752–763. [arXiv:astro-ph/9908035](https://arxiv.org/abs/astro-ph/9908035).
- Gadallah, K.A.K., Mutschke, H., Jäger, C., 2011. UV irradiated hydrogenated amorphous carbon (HAC) materials as a carrier candidate of the interstellar UV bump at 217.5 nm. *Astronomy and Astrophysics* 528, A56.
- Gadallah, K.A.K., Mutschke, H., Jäger, C., 2012a. Mid-infrared spectroscopy of UV irradiated hydrogenated amorphous carbon materials. *Astronomy and Astrophysics* 544, A107.
- Gadallah, K.A.K., Mutschke, H., Jäger, C., 2012b. UV-irradiated hydrogenated amorphous carbons (HACs) as carriers of the interstellar UV bump. *EAS Publications Series* 58, 389–393.
- Gadallah, K.A.K., Mutschke, H., Jäger, C., 2013. Analogs of solid nanoparticles as precursors of aromatic hydrocarbons. *Astronomy and Astrophysics* 554, A12.
- Goto, M., Gaessler, W., Hayano, Y., Iye, M., Kamata, Y., Kanzawa, T., Kobayashi, N., Minowa, Y., Saint-Jacques, D.J., Takami, H., Takato, N., Terada, H., 2003. Spatially Resolved 3 Micron Spectroscopy of IRAS 22272+5435: Formation and Evolution of Aliphatic Hydrocarbon Dust in Proto-Planetary Nebulae. *Astrophysical Journal* 589, 419–429. [arXiv:astro-ph/0301311](https://arxiv.org/abs/astro-ph/0301311).
- Goto, M., Maihara, T., Terada, H., Kaito, C., Kimura, S., Wada, S., 2000. Infrared spectral sequence of quenched carbonaceous composite subjected to thermal annealing. *Astronomy and Astrophysics, Supplement* 141, 149–156.
- Green, D.C., McKenzie, P.B., 1990. Properties and Characterization of Amorphous carbon films. *Mater. Sci. Forum* 52, 125.
- Grishko, V.I., Duley, W.W., 2002. Infrared Absorption and Emission Spectra of Hydrogenated Amorphous Carbon Prepared in the Presence of Oxygen, Nitrogen, Ammonia, and Carbon Monoxide. *Astrophysical Journal* 568, 448–453.
- Iida, Y., Yeung, E.S., 1994. Optical monitoring of laser-induced plasma derived from graphite and characterization of the deposited carbon film. *Appl. Spectrosc.* 48, 945–950.
- Jäger, C., Henning, T., Schlögl, R., Spillecke, O., 1999. Spectral properties of carbon black. *Journal of Non-Crystalline Solids* 258, 161 – 179.
- Jäger, C., Mutschke, H., Henning, T., 1998. Optical properties of carbonaceous dust analogues. *Astronomy and Astrophysics* 332, 291–299.
- Jäger, C., Mutschke, H., Henning, T., Huisken, F., 2008. Spectral Properties of Gas-phase Condensed Fullerene-like Carbon Nanoparticles from Far-ultraviolet to Infrared Wavelengths. *Astrophysical Journal* 689, 249–259. [0903.0759](https://arxiv.org/abs/0903.0759).

- Li, F., Lannin, J.S., 1990. Radial distribution function of amorphous carbon. *Physical Review Letters* 65, 1905 – 1908.
- Marchon, B., Salmeron, M., Siekhaus, W., 1989. Observation of graphitic and amorphous structures on the surface of hard carbon films by scanning tunneling microscopy. *Phys. Rev. B* 39, 12907–12910.
- Mennella, V., Colangeli, L., Blanco, A., Bussoletti, E., Fonti, S., Palumbo, P., Mertins, H.C., 1995. A dehydrogenation study of cosmic carbon analogue grains. *Astrophysical Journal* 444, 288–292.
- Mikhailov, E.F., Valsenko, S.S., Kiselev, A.A., 2001. Optics and structure carbonaceous soot aggregates. In: *Optics of Nanostructured Materials*, edited by V. A. Markel and T. F. George. John Wiley and sons, Inc., Chichester, UK, 2001 , p.413.
- Miyajima, Y., Henley, S.J., Adamopoulos, G., Stolojan, V., Garcia-Caurel, E., Drevillon, B., Shannon, J.M., Silva, S.R.P., 2009. Pulsed laser deposited tetrahedral amorphous carbon with high sp³ fractions and low optical bandgaps. *Journal of Applied Physics* 105, 073521 –073521–8.
- Mutsukura, N., Inoue, S., Machi, Y., 1992. Deposition mechanism of hydrogenated hard-carbon films in a CH₄ rf discharge plasma. *Journal of Applied Physics* 72, 43–53.
- Pan, H., Pruski, M., Gerstein, B.C., Li, F., Lannin, J.S., 1991. Local coordination of carbon atoms in amorphous carbon. *Phys. Rev. B* 44, 6741–6745.
- Phillips, J.C., 1979. *Structure of amorphous (Ge, Si)_{1-x}Y_x alloys*. *Physical Review Letters* 42, 1151–1154.
- Robertson, J., 1991. Hard amorphous (diamond-like) carbons. *Progress in Solid State Chemistry* 21, 199 – 333.
- Robertson, J., O'Reilly, E.P., 1987. Electronic and atomic structure of amorphous carbon. *Phys. Rev. B* 35, 2946–2957.
- Schnaiter, M., Mutschke, H., Dorschner, J., Henning, T., Salama, F., 1998. Matrix-isolated Nano-sized Carbon Grains as an Analog for the 217.5 Nanometer Feature Carrier. *Astrophysical Journal* 498, 486–498.
- Zubko, V.G., Mennella, V., Colangeli, L., Bussoletti, E., 1996. Optical constants of cosmic carbon analogue grains - I. Simulation of clustering by a modified continuous distribution of ellipsoids. *Monthly Notices of the RAS* 282, 1321–1329.